Fast intracavity polarization dynamics of an erbium-doped fiber ring laser: Inclusion of stochastic effects

Q. L. Williams, J. García-Ojalvo,* and R. Roy
School of Physics, Georgia Institute of Technology, Atlanta, Georgia 30332-0430
(Received 5 September 1996; revised manuscript received 31 October 1996)

The dynamics of a unidirectional erbium-doped fiber laser is investigated on a time scale short enough to observe, with good resolution, its behavior for individual round-trips in the laser cavity. With an intracavity polarization controller, a rich variety of nonlinear phenomena, ranging from self-pulsing to square-wave antiphase patterns in two orthogonal states of polarization, are observed. These patterns evolve continuously in time. A stochastic delay-differential equation model is proposed to describe this system. Numerical simulations show that this model satisfactorily accounts for all types of qualitative behavior and reveal that the inclusion of spontaneous-emission noise is necessary to reproduce the observed continuous pattern evolution. Two different, typical types of nonlinear dynamical states are found both numerically and experimentally: a deterministic, low-dimensional regime and a noise-driven high-dimensional motion. [S1050-2947(97)01403-0]

PACS number(s): 42.65.Sf, 42.81.−i

I. INTRODUCTION

The idea of doping glass to obtain amplifying optical fibers is very attractive from both a technological and a fundamental point of view. Technologically, fiber amplifiers are very promising useful devices in all-optical telecommunication schemes, through their use to replace repeaters in fiber-optic transmission lines, for instance. When these materials are complemented with a cavity resonator and a pumping scheme, laser emission can be obtained. Such systems are used for the generation of ultrashort pulses and solitons.

Besides their evident practical applications, fiber lasers are very interesting from a basic physics perspective. The conjunction of the inherent nonlinear character of both the optical fiber and the light amplification process makes this type of laser specially suited for investigations of nonlinear dynamics in optical systems. Furthermore, because of the amorphous character of the glass host, fiber lasers are the ideal counterpart of the more extended and well-known doped-crystal solid-state lasers.

Due to the optical-guiding characteristics of their amplifying medium, fiber lasers can have cavity lengths of the order of tens of meters, orders of magnitude higher than in most other lasers. This fact, along with the broad gain profile of doped fibers, ensures that a large number of longitudinal modes experience gain and coexist inside the cavity, coupled through gain sharing. Hence fiber lasers usually operate in a strongly multimode regime. The dynamics of multimode lasers is very rich, including antiphase behavior and self-organized collective oscillations [1]. Previous experiments in fiber lasers [2,3] have shown this kind of phenomenon in the dynamics of two orthogonal states of polarization, which suggest a description of this system in terms of two supermodes associated with two different polarization eigenstates of the field. Another dynamical feature that is usually observed in experiments is self-pulsing [4], which has recently been related to an absorption effect due to interaction between dopant ions [5]. All the previous experiments have been done in the millisecond to microsecond time scale, which corresponds to the relaxation-oscillation frequency of the laser. But this system, due to its large cavity length and thus long round-trip time, gives us a unique chance to observe its dynamics for individual round-trips inside the cavity. This work aims at the characterization of this fast polarization dynamics in the regimes previously mentioned.

We report experimental observations of the intracavity dynamics of an erbium-doped fiber laser. A polarization-controlling device has been included in the cavity and, as a result, a fast polarization-switching effect, on a time scale of the order of nanoseconds, has been observed. This kind of effect is known to occur in semiconductor lasers [6] when a wave plate is inserted in the laser cavity. Recently, optical feedback has been found to induce this effect also in Nd-doped fiber lasers [7], but on a much slower time scale (on the order of microseconds). A model is proposed to explain the behavior observed. Most models used so far in doped-fiber lasers to account for antiphase [2], self-pulsing [3], and polarization-switching [7] behavior are based on semiclassical rate equations for each of the two polarization supermodes, which are coupled to one another through cross saturation and gain sharing. In some cases, the need of explicitly taking into account the dependence of the system variables on the propagation direction has been stressed [3]. This consideration, which is, in general, advisable in this system due to its long cavity, is in our case unavoidable given the time scale in which the observations are made. Following Loh and Tang [8,9] in their modeling of fast polarization self-modulation in semiconductor lasers, we develop a delay-differential equation model that accounts for all kinds of features observed. The inclusion of spontaneous-emission noise is seen to be necessary to obtain a more complete agreement. Indeed, the importance of spontaneous emission in the dynamics of guided lasers is a well-established fact [2]. Finally,

*Permanent address: Departament de Física i Enginyeria Nuclear, Escola Tècnica Superior d'Enginyers Industrials de Terrassa, Universitat Politècnica de Catalunya, Colom 11, E-08222 Terrassa, Spain.

 © 1997 The American Physical Society

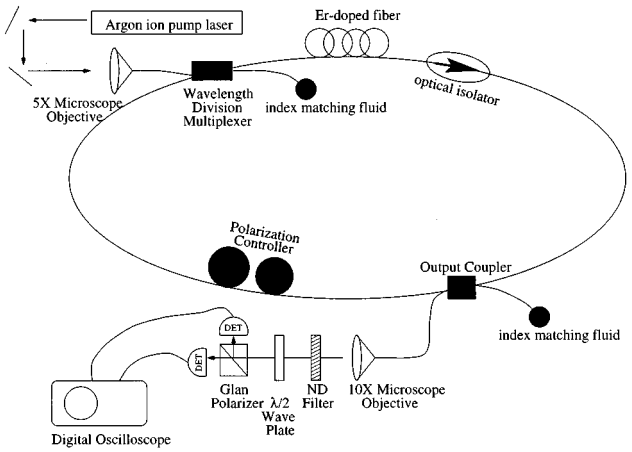

FIG. 1. Experimental setup.

in order to simplify the modeling of the system, a ring-cavity configuration is used. Preliminary results of this investigation have been reported elsewhere [10].

The outline of the paper is the following. Section II contains a description of the experimental apparatus and a report of the behavior observed. Section III establishes a theoretical model that reproduces this behavior, as shown by numerical simulations. Finally, some conclusions and comments are made in Sec. IV.

II. EXPERIMENTAL FEATURES

A. Experimental setup

Several wavelengths can be used to optically pump an erbium-doped fiber amplifier in order to obtain laser emission. In our case the pump wavelength is fixed at 514.5 nm and is provided by an Ar^+-ion laser. Under these conditions, the lasing frequency lies in the near infrared, at 1.561μm. The experimental setup is shown in Fig. 1. The amplifying medium is a 6-m-long erbium-doped fiber, with an ion concentration of approximately 240 ppm (corresponding to 4.98×10^{25} ions/m^3). The total cavity length is made to be 20 m long with the addition of 14 m of passive optical fiber. The fiber is closed on itself in order to form a ring cavity. To ensure unidirectional operation, an optical isolator is placed inside the cavity. The optical isolator is based on the Faraday effect and is polarization insensitive. The pump light coming from the argon laser is launched into the ring fiber through a wavelength division multiplexer (WDM), while an output coupler removes part of the light that circulates inside the cavity. In both cases, fiber ends were placed in an index-matching fluid to prevent possible parasitic Fresnel reflections, as shown in Fig. 1. Two different output couplers have been used, with coupling ratios 90/10 (10%) and 97/3 (3%), respectively. A $5\times$ microscope objective is used to optimize the coupling of the pump light into the input port of the WDM. The output emission is passed through a 10% transmission neutral density (ND) filter and a half-wave plate to a polarization beam splitter, which separates the light into its two orthogonal polarization components. These components are measured with two high-speed photodetectors connected to the two input channels of a fast digital oscilloscope with a 1-GHz sampling rate. This setup allows us to measure the intensity with 100 data points per cavity round-trip.

In order to modify the polarization state of the light traveling inside the fiber, a polarization controller is used. Polarization controllers produce a phase shift by introducing a local birefringence into a portion of the fiber. This is accomplished by winding the fiber around mandrels of the proper diameter. It is very important to correctly choose both the diameter of the mandrels and the number of turns of the fiber around them: if the diameter is too small, the bending loss of the device becomes too high; too few turns would undesirably reduce the phase shift. We found that, for wavelengths of the circulating light, a diameter of 38 mm and three turns of fiber around each mandrel was a good choice to produce a small loss and a retardation effect similar to that of a half-wave plate.

B. Characterization of the system

A measurement of the total output power as a function of pumping is the first standard procedure used to characterize this laser system. Such a procedure shows that the lasing threshold is $\sim$150 mW. When the the output light is separated into its two orthogonal polarization components, one can see that the two states have slightly different thresholds and very different output vs pump slopes in the lasing regime. This is a first indication of the well-known two-mode-like behavior of doped-fiber lasers [2,3]. By suitably modifying the state of the polarization controller, it is possible to separate the two main groups of modes that are amplified inside the cavity. The optical spectra in two orthogonal polarization directions, as obtained from an optical spectrum analyzer, show that the two mode groups are indeed orthogonal and linearly polarized, with spectral peaks centered around $\sim1.560\,52$ μm and $\sim1.561\,05$ μm, respectively.

The behavior of output vs pump power in the lasing regime is observed to be linear, which is a characteristic of most lasers. Nevertheless, at high pump powers, an increase of output power fluctuations occurs while making the measurements. In order to quantify this effect, one can measure the standard deviation of these fluctuations as a function of the mean light intensity and pump power. The results are shown in Fig. 2 for the case of 10% output coupling. For the sake of clarity, we should remark at this point that the pump power that appears in this figure is just the recorded output of the pump laser; it does not correspond exactly to the actual power that is being injected into the fiber laser, due to the imperfect launching of pump light into the cavity through the WDM. In any case, an analysis of this figure reveals a steady increase of the fluctuations as both pump level and output power are raised. This phenomenon is rather unexpected; in most single mode lasers, fluctuations produced by spontaneous emission are independent of pump level once lasing has been achieved. This is so because the spontaneous-emission rate is proportional to the population inversion in the amplifying medium, and this is constant beyond threshold, as can be seen from any rate-equation model [11]. In multimode lasers, these fluctuations may be deterministic and originate in the nonlinear dynamics of modes coupled through sharing of the population inversion.

We can calculate the number of modes inside the cavity by measuring the optical spectrum of the output light. The ratio of its full width at half maximum to the free spectral

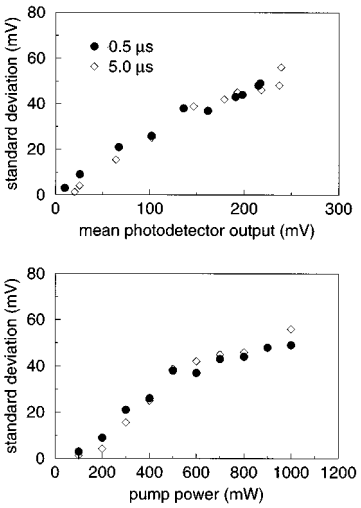

FIG. 2. Standard deviation of the output intensity fluctuations vs the mean output level and pump power. Two different sample times (shown in the legend) have been used. The pump power shown in the lower figure does not correspond to the power that is actually injected into the fiber.

range of the cavity (longitudinal mode spacing) gives us an estimate of this quantity. We observe a pronounced spectral narrowing and a corresponding sharp decrease in the number of modes (from $\sim 3\times 10^5$ to $\sim 2\times 10^3$) as the lasing threshold is crossed. Note, however, that even in the lasing regime the number of amplified modes is very large. This fact shows the strongly multimode character of fiber lasers.

C. Dynamical behavior

1. Self-pulsing

A characteristic time trace of the total output intensity extracted by the output coupler in the higher loss case (10% coupling) is shown in Fig. 3 for a pump rate well above threshold. Self-pulsing is observed with a periodicity of ~ 100 ns. This corresponds to the cavity round-trip time of our system, which is estimated as L/v, where $L=20$ m is the cavity length and $v=c/n$ is the speed of light in the fiber. The index of refraction of erbium-doped fiber is $n=1.46$.

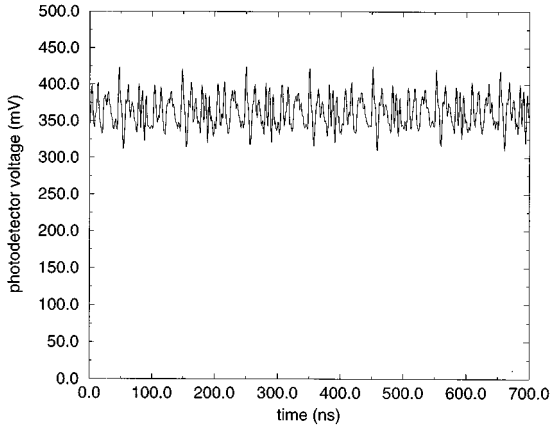

FIG. 3. Total output intensity time trace showing self-pulsing with 10% output coupler. The pump power is 400 mW.

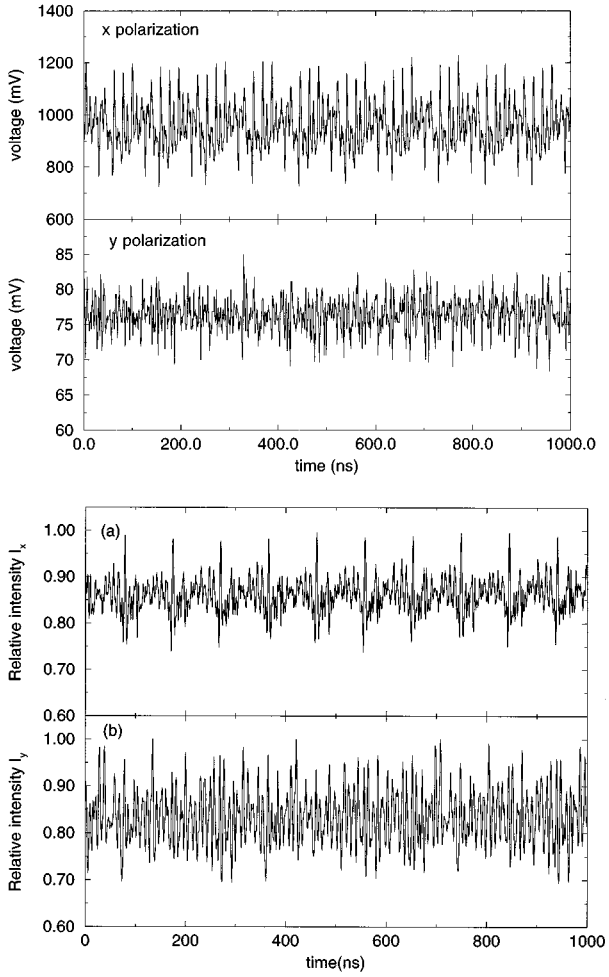

FIG. 4. Two different polarization-resolved time traces. Both polarization directions are shown in each case.

One can now resolve the output in terms of its orthogonal linear polarization components. These components, although coupled, may exhibit very different dynamics. Figure 4(a) shows quasiperiodic behavior in one polarization direction and random evolution in the other, also for 10% output coupling. In other experimental situations, one can observe different quasiperiodic evolution in the two modes. Figure 4(b) corresponds to a case with period-1 behavior in one direction and period-7 in the other. The 3% output coupler has been used in this case.

2. Influence of the polarization controller

Another way of establishing the distinct character of the polarization-resolved intensity time traces compared to those of the total output intensity is through their power spectrum. In the latter case, a typical spectrum shows peaks separated by the fundamental cavity frequency of 9.8 MHz. However, when the signal used comes from a single polarization direction, sideband peaks appear between the main ones. These sidebands can be tuned by manipulating the polarization controller and eventually can be made to overlap. When this happens and losses are small enough (i.e., the light intensity inside the cavity is high enough), the pulsed behavior disappears and square pulses develop in the output intensity of the

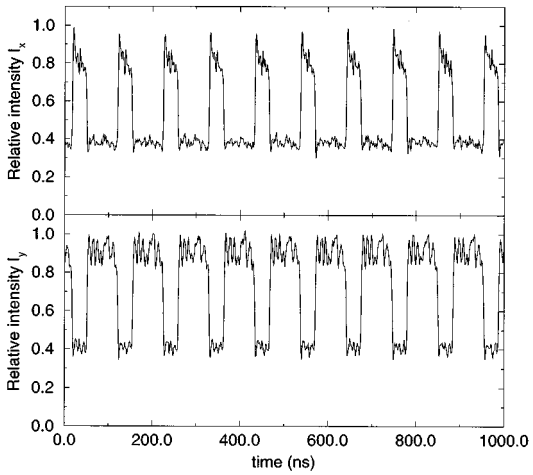

FIG. 5. Antiphase square pulsing in the two orthogonal polarization components of the output light for a given setting of the polarization controller and a 3% output coupling. The pump power is 600 mW.

orthogonal polarization states. This behavior is antiphase in the two states and is periodic at the cavity round-trip time, as shown in Fig. 5. The requirement that losses have to be low for this effect to occur is reflected in the fact that square pulses are observed when the 3% output coupler is used, but not in the 10% case. It is also worth noting that the time durations of the plateaus correspond to the lengths of the active and passive part of the fiber. In other words, the 70-ns upper part of the pulse in the *y*-polarization trace of Fig. 5 corresponds to the 14 m of passive fiber, whereas the 30-ns lower part is related to the 6 m of active erbium-doped fiber. A threshold pump power is typically observed for the onset of square pulsing. For the measurements shown, square pulses formed at a pump power ~ 2.2 times above threshold. In addition to square pulses, other antiphase pulse patterns have been observed. One of them is shown in Fig. 6. A final remark on this behavior is that the irregular intensity patterns superimposed on the plateaus of the square waves evolve continuously and slowly in time.

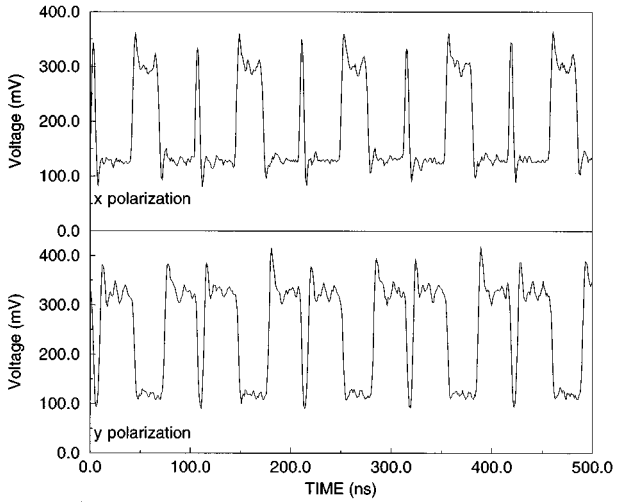

FIG. 6. Another antiphase pattern observed. Here the pump power is here 700 mW.

D. Nonlinear analysis

We have observed so far that this system has a wide variety of nonlinear attractors: regular or irregular temporal patterns in which the dynamics are trapped. Which specific attractor occurs depends on many factors: the state of the polarization controller, the pump power, the output losses, etc. We are now interested in dynamical characteristics of these attractors.

The state space of a dynamical system can be reconstructed from the information obtained through a scalar measurement (the intensity of one of the polarization eigenstates, for instance) by means of time-delay vectors [12]. If we denote as $x(n) \equiv x(t_0 + n\Delta)$ a scalar set of measurements sampled at equally spaced time intervals Δ, one can construct d-dimensional vectors

$$\mathbf{y}(n) = (x(n), x(n+T), \ldots, x(n+[d-1]T)). \qquad (1)$$

The evolution of these time-delayed vectors in state space describes an attractor. There exists a minimum value of d for this attractor to properly represent the dynamical behavior of the system. This value is called the *embedding dimension* of the system. Both the embedding dimension and the time lag T have to be chosen carefully if one wants this state space reconstruction to be really useful.

To obtain a reasonable value of the time delay T, one has to reach a compromise between the high correlation between vector components that would arise if T is chosen too small [$x(n+iT)$ and $x(n+(i-1)T)$ would be nearly identical] and their statistical independence if T is too large. All these features are reflected in the so-called *average mutual information function*, which can be interpreted as a nonlinear correlation function between the time series $x(n)$ and $x(n+\Delta t)$ as a function of the time lag Δt. Its definition is

$$M(\Delta t) = \sum_{n=1}^{N} P(s(n), s(n+\Delta t)) \times \log_2 \left[\frac{P(s(n), s(n+\Delta t))}{P(s(n)) P(s(n+\Delta t))} \right], \qquad (2)$$

where $P(s(n))$ is the probability density of the process $s(n)$ and $P(s(n), s(n+\Delta t))$ is the joint probability of the two time-shifted series. A high value of this function represents a high correlation between the series and a low value corresponds to a high degree of independence. A suitable value of T will be intermediate between these two regimes. A reasonable prescription that is frequently used [13] is to choose T as the first minimum of $M(\Delta t)$.

We can compute the average mutual information function (2) for the time series measurements obtained from our experiment. A typical result is shown in Fig. 7, corresponding to the intensity for a single polarization direction. The behavior is roughly the same for the other polarization direction and for the total output and also for the other different dynamical regimes investigated. The results suggest that an adequate value for the time delay is $T = 3$.

Once the time delay has been chosen, one needs to determine the embedding dimension. To do so, we use a method proposed in Ref. [14]. This procedure determines the minimum useful embedding dimension as that for which the per-

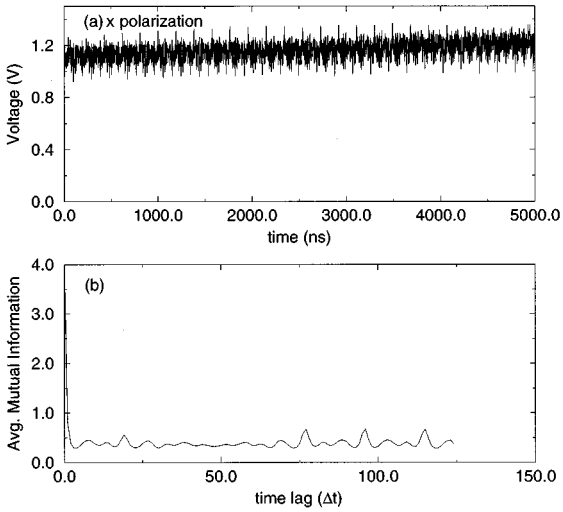

FIG. 7. Self-pulsing time series for the intensity output in one of the polarization directions and its corresponding average mutual information function. The pulse separation is $2\tau_R$ and the pump power is 1000 mW.

centage of *false nearest neighbors* (FNNs) in the attractor drops to zero. Two points of the attractor are said to be FNNs when they seem to be close only because the attractor is embedded in a dimension that is too low, but they are actually separated from one another. They can be identified by measuring the distance between them in two consecutive dimensions. When this distance is very small in the lowest-dimensional space and much larger in the highest-dimensional space, the two points are FNNs. The procedure consists of computing the percentage of FNNs for increasing dimensions. The embedding dimension is then determined as that dimension for which this percentage drops to a very small number. Figure 8 presents the result of this method for two different time series exhibiting very different dynamical behaviors. Figure 8(a) corresponds to a quasiperiodic low-dimensional regime with an embedding dimension $d_E=4$. Figure 8(b), on the other hand, shows a nonperiodic time series whose percentage of FNNs does not go to zero as the embedding dimension increases. This indicates that the dynamics in this case is high dimensional and hence noise driven. A similar coexistence of deterministic and stochastic behavior in the same dynamical system has recently been observed in a Nd:YAG laser (where YAG denotes yttrium aluminum garnet) exhibiting deterministic chaos [15].

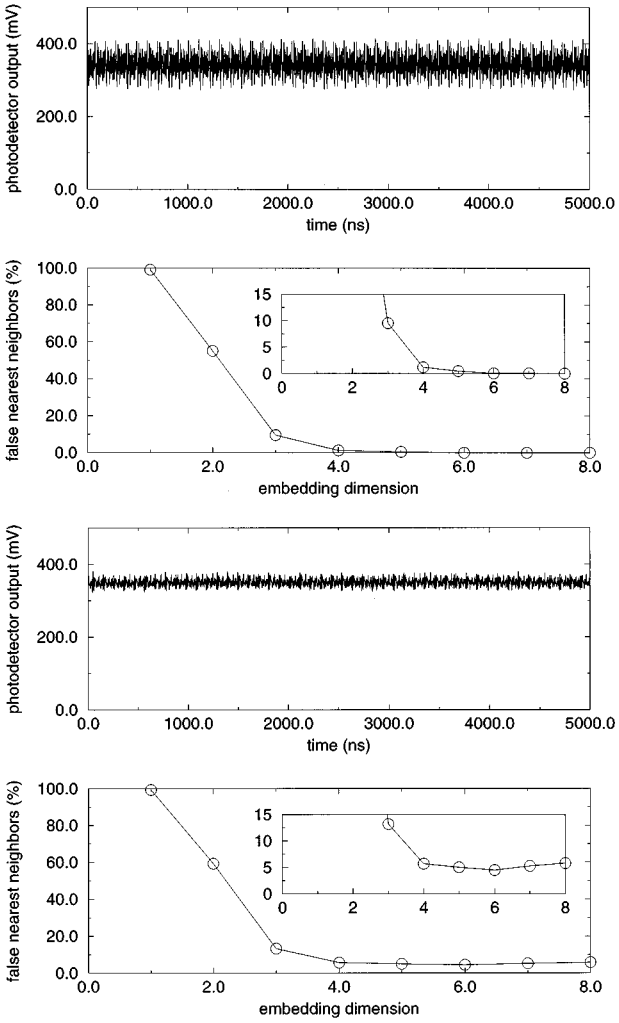

FIG. 8. Experimental time traces and the corresponding percentage of false nearest neighbors vs dimension for the (a) quasiperiodic case and (b) nonperiodic case. The insets in the lower plots show a zoom of the relevant regions of the graph.

III. MODELING

A. A delay-differential equation model

To develop a theoretical model that reproduces the observations made so far, several important characteristics of this system have to be taken into account.

(i) Even though many longitudinal modes are being amplified inside the cavity, the dynamics of the system can be described in terms of two supermodes corresponding to two orthogonal polarization states of the emitted light [2,3,7].

(ii) A description in terms of two-level rate equations is not suitable because of the long cavity of fiber lasers [3]. Variations in the direction of propagation of laser light have to be taken into account. This requirement is completely unavoidable in our case since we are observing the dynamics *within* individual cavity round-trips.

(iii) The polarization controller is acting as an imperfect half-wave plate that almost completely switches polarizations once every cavity round-trip.

(iv) Only part of the total cavity length is active medium. Hence this system has two different characteristic lengths which are reflected in the experimental results (see Sec. II C 2) and must appear also in the theoretical model.

(v) Spontaneous-emission noise is known to have an important influence on the behavior of guided lasers such as the one we are dealing with in this experiment [2]. It thus seems necessary to include it in any realistic model of fiber lasers.

The first three points in the previous list have already been faced by Loh and Tang [8,9] in their description of ultrafast polarization self-modulation in semiconductor lasers. In this study, they developed a delay-differential equation model similar in approach to that used by Ikeda and co-workers [16,17] to analyze instabilities in the absorption of light by a passive medium placed inside a ring cavity and

by Otsuka and Iwamura [18] to model the dynamics of semiconductor laser amplifiers. We will follow the spirit of Loh and Tang's study to derive a model for our system.

Let $E_1(t,z)$ and $E_2(t,z)$ be the complex field envelopes of the two polarization modes of the amplified radiation. The following set of equations can be derived for their time evolution after adiabatically eliminating the polarization of the medium from the corresponding Maxwell-Bloch equations [8]:

$$\frac{\partial E_1(t,z)}{\partial z}+\frac{1}{v_g}\frac{\partial E_1(t,z)}{\partial t}=\frac{a_1}{2}(1-i\alpha_1)[N-N_0]E_1(t,z)+\mu_1(t,z), \tag{3}$$

$$\frac{\partial E_2(t,z)}{\partial z}+\frac{1}{v_g}\frac{\partial E_2(t,z)}{\partial t}=\frac{a_2}{2}t(1-i\alpha_2)[N-N_0]E_2(t,z)+\mu_2(t,z), \tag{4}$$

$$\frac{\partial N(t,z)}{\partial t}=P-\gamma_{||}[N(t,z)+N_t]-a_1[N(t,z)-N_0]\frac{|E_1|^2}{\hbar\omega_1}-a_2[N(t,z)-N_0]\frac{|E_2|^2}{\hbar\omega_2}. \tag{5}$$

It can be seen that the two modes are coupled through $N(t,z)$, the population inversion of the medium. N_0 is the population inversion necessary for transparency (i.e., for zero gain) and N_t the density of erbium ions in the fiber. The quantity N_t has to be taken into account because erbium-doped fiber, when pumped at 514.5 nm, behaves as a three-level medium with incoherent pumping [11]. a_1 and a_2 are gain coefficients, α_1 and α_2 represent the detuning between the corresponding mode frequency ω_i and the resonance frequency of the cavity ω_0 [$\alpha_i=(\omega_0-\omega_i)/\gamma_\perp$, where $\gamma_\perp$ is the decay rate of the polarization of the medium], v_g is the velocity of light in the medium (assumed equal for the two modes), and P is the pump rate. These parameters have been defined in Ref. [10]. z is the direction of propagation of the light inside the cavity. $\mu_1(t,z)$ and $\mu_2(t,z)$ are spatiotemporal Gaussian and white stochastic processes that account for spontaneous emission. They have zero mean and correlation given by

$$\langle\mu_i(t,z)\mu_j^*(t',z')\rangle=2D_i\delta_{ij}\delta(t-t')\delta(z-z'). \tag{6}$$

We are now going to map the spatial dependence of the system into time by making use of the boundary conditions that have to be fulfilled by the fields E_1 and E_2 inside the cavity. These boundary conditions are

$$E_1(t,0)=\frac{1}{2}R_1e^{ik_1L}\left[E_1\left(t-\frac{l_P}{v_g},l_A\right)(e^{i\varphi}+1)+E_2\left(t-\frac{l_P}{v_g},l_A\right)(e^{i\varphi}-1)e^{-i\beta}\right], \tag{7}$$

$$E_2(t,0)=\frac{1}{2}R_2e^{ik_2L}\left[E_1\left(t-\frac{l_P}{v_g},l_A\right)(e^{i\varphi}-1)+E_2\left(t-\frac{l_P}{v_g},l_A\right)(e^{i\varphi}+1)e^{-i\beta}\right]. \tag{8}$$

Here l_A and l_P are the lengths of the active and passive parts of the fiber, respectively, and $L=l_A+l_P$ is the total fiber length. The reference frame is chosen in such a way that $z=0$ corresponds to one end of the active fiber. R_1 and R_2 are the return coefficients of the output coupler for each one of the modes. The parameter φ represents the phase shift caused by the polarization controller. In the perfect half-wave case ($\varphi=\pi$) it can be seen that the previous boundary conditions merely represent an exchange of polarizations every round-trip. We shall consider φ near, but not equal to, its perfect half-wave value. Finally, the parameter β represents the birefringence of the fiber, which causes different phase shifts in the two polarization modes. These different phase shifts are produced by the different velocities that the two modes actually have when traveling through the fiber, which can be modeled satisfactorily by including the parameter β while keeping v_g equal in both modes [9].

The previous boundary conditions can be used in combination with an integration of Eqs. (3)–(5) with respect to z to obtain the difference-differential model [9,19]

$$\psi_1(t)=\frac{1}{2}R_1\Lambda_1\left\{\left[\psi_1(t-\tau_R)\exp\left(\frac{\Gamma_1}{2}(1-i\alpha_1)[\phi(t)-1]\right)+\eta_1(t)\right](e^{i\varphi}+1)\times\left[\psi_2(t-\tau_R)\exp\left(\frac{\Gamma_2}{2}(1-i\alpha_2)[\phi(t)-1]\right)+\eta_2(t)\right](e^{i\varphi}-1)e^{-i\beta}\right\}, \tag{9}$$

$$\psi_2(t)=\frac{1}{2}R_2\Lambda_2\left\{\left[\psi_1(t-\tau_R)\exp\left(\frac{\Gamma_1}{2}(1-i\alpha_1)[\phi(t)-1]\right)+\eta_1(t)\right](e^{i\varphi}-1)\times\left[\psi_2(t-\tau_R)\exp\left(\frac{\Gamma_2}{2}(1-i\alpha_2)[\phi(t)-1]\right)+\eta_2(t)\right](e^{i\varphi}+1)e^{-i\beta}\right\}, \tag{10}$$

$$\frac{\partial\phi}{\partial t}=q-\phi(t)-|\psi_1(t-\tau_R)|^2(\exp\{\Gamma_1[\phi(t)-1]\}-1)-\mathrm{Re}[\psi_1(t-\tau_R)\xi_1(t)]-|\psi_2(t-\tau_R)|^2(\exp\{\Gamma_2[\phi(t)-1]\}-1)-\mathrm{Re}[\psi_2(t-\tau_R)\xi_2(t)], \tag{11}$$

where new dimensionless variables have been defined. ψ_1 and ψ_2 are related to the electric field envelopes at $z=0$,

$$\psi_i(t) \equiv \frac{E_i(t,0)}{\sqrt{\hbar \omega l_A \gamma_{||} N_0}} \tag{12}$$

and ϕ is the dimensionless total population inversion in the active fiber,

$$\phi(t) \equiv \frac{W(t-\tau_R, l_A)}{l_A N_0} = \frac{1}{l_A N_0} \int_0^{l_A} N(t-\tau_R, z)\, dz. \tag{13}$$

Time is now measured in units of $\gamma_{||}^{-1}$. τ_R is the cavity round-trip time, also measured in units of $\gamma_{||}^{-1}$ ($\tau_R = L/v_g \gamma_{||}$). We have defined a dimensionless gain parameter and an effective pump rate as

$$\Gamma_i = a_i l_A N_0, \quad q \equiv \frac{P}{\gamma_{||} N_0} - \frac{N_t}{N_0}. \tag{14}$$

Λ_1 and Λ_2 are phase-shift coefficients that can be evaluated as [9]

$$\Lambda_i \equiv e^{ik_i L} = \exp\left[i \alpha_i \frac{\Gamma_i}{2} [\phi(0) - 1] \right]. \tag{15}$$

An inspection of the delay-differential model (9)–(11) shows that the original spontaneous emission noise sources $\mu_i(t,z)$, $i=\{1,2\}$, have given rise to new noise terms $\eta_i(t)$ and $\xi_i(t)$ in all three equations for the electric fields and the population inversion. The stochastic processes $\eta_i(t)$ come from the formal integration of the spontaneous-emission noise sources $\mu_i(t,z)$ over the space variable z, whereas $\xi_i(t)$ appear through the introduction of the result of this integration into Eq. (5). It is worth noting that these new stochastic processes are no longer space dependent; this is true of all the other quantities of the model as well. Note also that in the population inversion equation the noise terms are *multiplicative* [19]. They are all Gaussian distributed with zero mean, and we will denote their variances by D_i^{η} and D_i^{ξ}. We will treat these noise strengths as adjustable parameters for our studies; they can be related to the physical properties of the system as [19]

$$D_i^{\eta} = \frac{D_i}{\hbar \omega_i N_0},$$

$$D_i^{\xi} = 4\, a_i^2 (N_{\mathrm{SS}} - N_0)^2 l_A^2 \frac{D_i}{\hbar \omega_i N_0}, \tag{16}$$

where N_{SS} is the steady-state value of the population inversion.

In summary, we have obtained a delay-differential equation model that translates the space dependence on the propagation direction z (and hence its infinite-dimensional character) into a dependence on time-delayed quantities. The model also includes the influence of intrinsic noise sources. We have performed extensive numerical computations with this model, and the results obtained will be described in the following subsections.

The simulations are performed as follows. Each cavity round-trip time is divided into equal-size time intervals (or, equivalently, the cavity is discretized in a number of equal cells). The evolution of the fields ψ_1 and ψ_2 depends on their values one round-trip earlier [Eqs. (9) and (10)] and the total inversion ϕ evolves according to the differential equation (11), which is discretized in the equally spaced time intervals defined above (or in the one-dimensional spatial lattice in which the cavity has been divided). Since in our case the cavity round-trip time is much smaller than the population inversion decay time, the integration time steps resulting from a not very dense cavity subdivision are small enough to ensure numerical stability in the algorithm that integrates the differential equation. We will usually choose a subdivision of the cavity in 100 parts and use a Heun algorithm (a stochastic version of a second-order Runge-Kutta scheme) [20] to simulate that equation. The multiplicative noise terms are treated according to a Stratonovich interpretation.

A distinction has to be made at this point between the active and the passive fiber. Since the polarization controller is located in the passive part of the cavity and the delay differential model maps time into space, the value of the phase shift φ will be close to π only in the time instants corresponding to the passive part of the fiber. The rest of the time φ will be near zero (not exactly zero because any small winding in the active fiber may also have a small phase-shifting effect). Hence we will take φ to be equal to φ_A (small) in the active region and to φ_P (close to π) in the passive part.

Several of the parameters of the model will be fixed by physical requirements of the active medium and the experimental setup, whereas others will be used as adjustable parameters. Among the former, we have the gain coefficients a_1 and a_2, which will be taken to be coincident and equal to 2.03×10^{-23} m^2. The detuning factors α_1 and α_2 will also be chosen to be the same and equal to 3.52×10^{-2}. The population decay rate $\gamma_{||}$ is 10^2 s^{-1} and its inverse is the time unit we use throughout this section. The lengths of the active and passive fibers are the ones used in the experiment (6 m and 14 m, respectively), with a total cavity length of $L=20$ m, which gives a round-trip time equal to $\tau_R = nL/c\,\gamma_{||} = 10^{-5}$ dimensionless time units. The dopant ion concentration is $N_t = 4.98\times10^{25}$ m^{-3} and the transparency inversion is $N_0 \approx 10^{20}$ m^{-3}. The return coefficient of the output coupler will be taken to be, according to the experimental setup, $R_1 = R_2 = 0.97$, equal for both polarization modes. The noise strengths are chosen to be $D_1^{\eta} = D_2^{\eta} = D_1^{\xi} = D_2^{\xi} = 10^{-5}$. To put these noise source variances in perspective, we should remark at this point that the magnitude of the light intensity in the lasing regime is, in our dimensionless units, of the order of 10^6. The pump rate will take several values for the different regimes. The phase shifts φ_A and φ_P and the birefringence coefficient β will be adjustable parameters. A summary of the previous values is shown in Table I.

B. Characterization of the model

A first comparison between the numerical model that has just been derived and the experimental observations shown previously is made by computing how the laser output

TABLE I. Parameters used in the delay-differential model.

Parameter	Value	Units	Description
$a_{1,2}$	2.03×10^{-23}	m^2	gain coefficients
$\alpha_{1,2}$	3.52×10^{-2}		detuning factors
$\gamma_{\|\|}$	10^2	s^{-1}	population decay rate
l_A	6	m	length of active fiber
L	20	m	total cavity length
τ_R	10^{-7}	s	cavity round-trip time
N_0	10^{20}	m^{-3}	transparency inversion
N_t	4.98×10^{25}	m^{-3}	dopant ion concentration
$R_{1,2}$	0.97		output coupler return
$D^{\eta}_{1,2}$	10^{-5}		coefficients
$D^{\xi}_{1,2}$	10^{-5}		electric-field noise strength
			population inversion noise strength

changes with increasing pump power. A sudden jump in photon number (over nine orders of magnitude) is observed and represents the transition from a spontaneous emission (no lasing) to a stimulated emission regime (lasing). Linear behavior is observed in the lasing regime. The estimated value of the lasing threshold ($\sim5\times10^5$ in dimensionless units) is in qualitative agreement with the experimental result.

It has also been found that this model reproduces the striking experimental observation of an increase in intensity fluctuations for higher pumping and output power. The results are shown in Fig. 9 and should be compared with their experimental counterpart presented in Fig. 4. The fact that this behavior persists even in the absence of stochastic terms in the simulations indicates that these intensity fluctuations are of deterministic origin. They are related to spiking and pulsing phenomena occurring in the time evolution of the light intensity and may be caused by the coupling dynamics between the many modes that are undergoing amplification, as mentioned in Sec. III A.

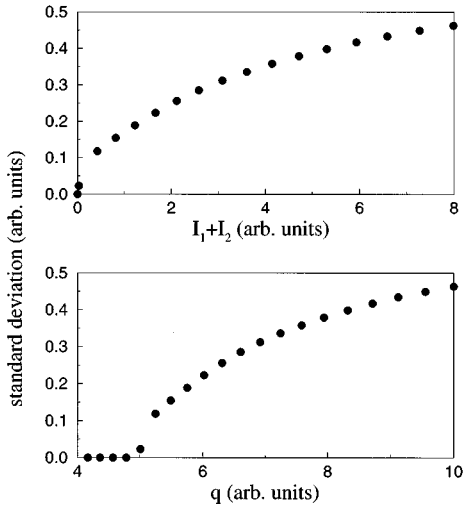

FIG. 9. Standard deviation of the total intensity output vs total output power I_1+I_2 and pump rate q.

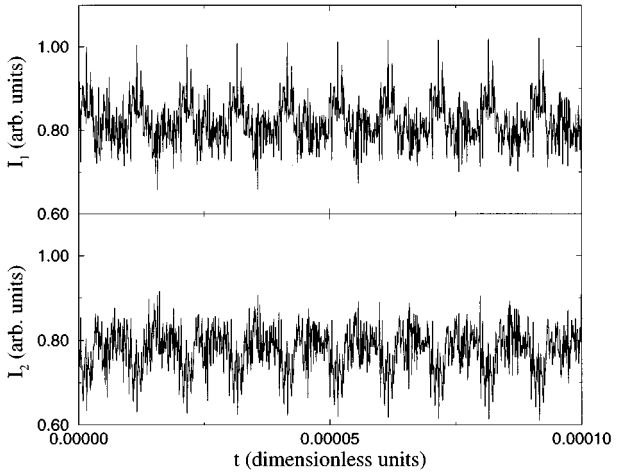

FIG. 10. Polarization-resolved quasiperiodic self-pulsing time traces. A periodicity equal to one cavity round-trip time is observed. The pump rate is $q=2\times10^6$ dimensionless units, roughly 5 times above threshold.

C. Dynamical behavior

1. Self-pulsing

Typical time traces of the output intensity $I_i=|\psi_i|^2$, as obtained from our delay-differential model, are shown in Figs. 10 and 11. Self-pulsing behavior is clearly observed, with different overall characteristics depending on the values of the parameters. Figure 10 presents antiphase quasiperiodic self-pulses at a periodicity of one cavity round-trip time. Figure 11 shows period-2 behavior. The difference between both cases lies only in the value of the birefringence factor, equal to 0.0015 in the first case and taken to be exactly zero in the second. The values chosen for the phase shifts are 0.027 in the active fiber and $\pi-0.175$ in the passive fiber. All the other parameters are those of Table I. It is worth noting that in all cases we obtain antiphase motion for the two polarization modes. The structures immersed in this self-pulsing behavior are observed to drift slowly as time

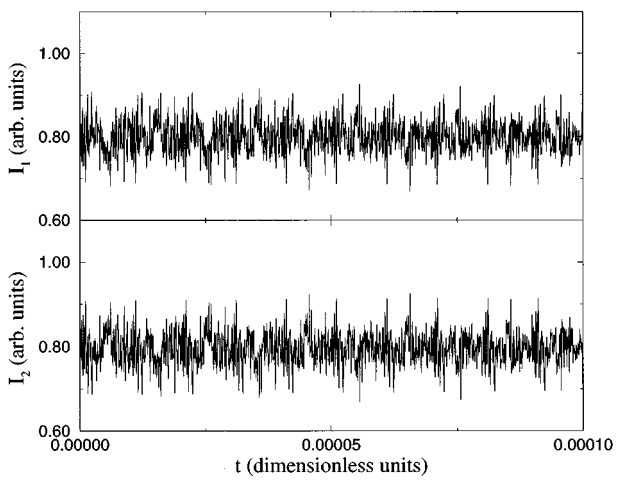

FIG. 11. Polarization-resolved quasiperiodic self-pulsing time traces with a period equal to $2\tau_R$. The pump rate is the same as in Fig. 10.

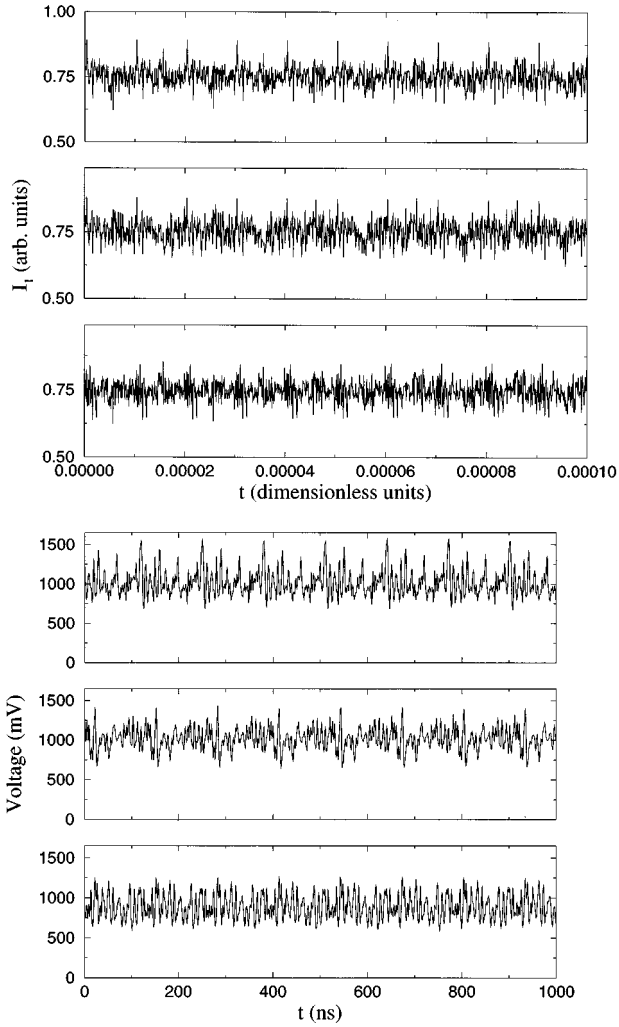

FIG. 12. Three snapshots of the self-pulsing behavior of one polarization mode, showing the slow drift of temporal patterns due to the effect of stochastic noise sources. These snapshots are separated in time by several hundred round-trips. (a) Numerical simulation (parameters are the same as in the previous figures) and (b) experimental behavior (in this case the cavity round-trip time is ~ 130 ns).

evolves, as observed in the experiments (see Fig. 12). This pattern evolution does not occur if the noise sources are neglected in the model, which indicates the importance of spontaneous emission in this system.

2. Influence of the phase shifts

The value of φ_P used in the previous simulations corresponds to an imperfect half-wave plate. By taking a value of this phase shift closer to π (which amounts to properly tuning the polarization-controller mandrels in the experiment), we can reproduce the square-wave behavior observed in the real system. Figure 13 is the result of making $\varphi_P = \pi - 0.015$ and $\beta = 0.020$. As in the experimental output, these square waves are antiphase in both polarization components, with a period equal to the cavity round-trip time, and a relation between the lengths of the upper and lower plateau equal to that between the lengths of the active and passive part of the cavity. Also, as in the experiment, the

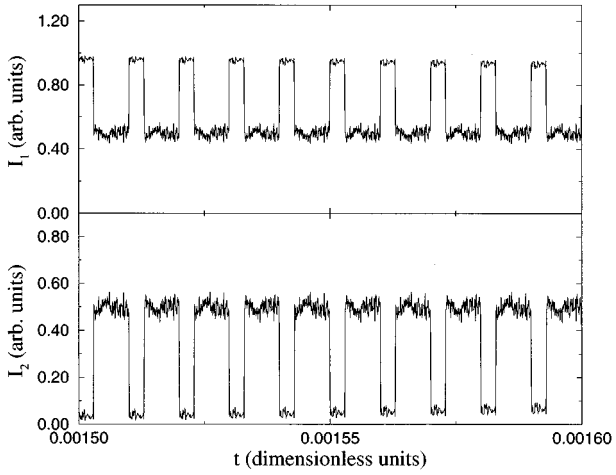

FIG. 13. Antiphase square pulses generated by the delay-differential model by properly tuning the value of φ_P. The pump rate is the same as in the previous figures.

patterns on top of the square pulses change continuously and slowly with time, as shown in Fig. 14, where three series of ten cavity round-trip times occurring at different instants of the same dynamical evolution are compared. Again, this behavior is not obtained if the spontaneous-emission noise is not taken into account.

D. Nonlinear analysis

To complete our comparison between the results given by the delay-differential model that has been derived in this section and the results obtained from the experimental system, we will analyze the numerical time traces from a nonlinear dynamics point of view. We can compute the average mutual information function of a polarization-resolved output time trace. Figure 15 shows the typical behavior of this function [which in this case corresponds specifically to the time trace shown in Fig. 16(a)]. We conclude that a reasonable value

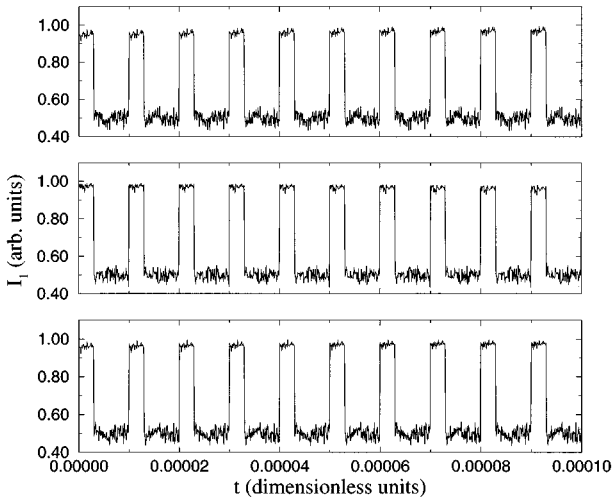

FIG. 14. Three snapshots of the numerically simulated behavior of one polarization mode, showing that the detailed structure of the square-wave patterns evolves slowly in time. The parameters are the same as in the previous figures.

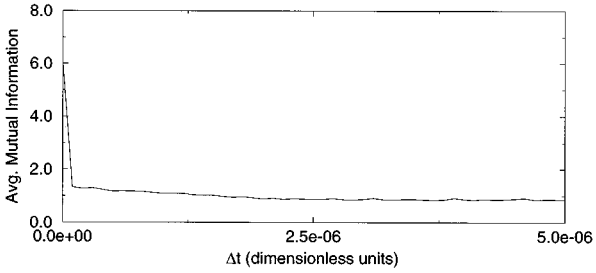

FIG. 15. Typical example of the average mutual information function obtained numerically. The actual time trace from which this function has been derived is shown in Fig. 16(a).

for the time lag to be used in phase-space reconstruction is $\Delta t = 10^{-7}$ dimensionless units, which corresponds to one time interval in the cavity subdivision we have chosen throughout this work. We now compute the percentage of false nearest neighbors for different dimensions in two different regimes. Figure 16(a) shows a time trace exhibiting a high degree of periodicity and its corresponding false-nearest-neighbor percentage vs embedding dimension. This result shows that the behavior of the system in this regime is low-dimensional and deterministic, with an embedding dimension $d_E = 4$. Figure 16(b), on the other hand, shows a nonperiodic time trace and a false-nearest-neighbor percentage that does *not* go to zero for increasing dimension, implying that the behavior in this case is high dimensional and noise driven. We remind the reader that these two different regimes have also been obtained experimentally (Fig. 8). We regard this agreement as a significant indication of the success of our model in capturing the dynamical behavior of the laser system.

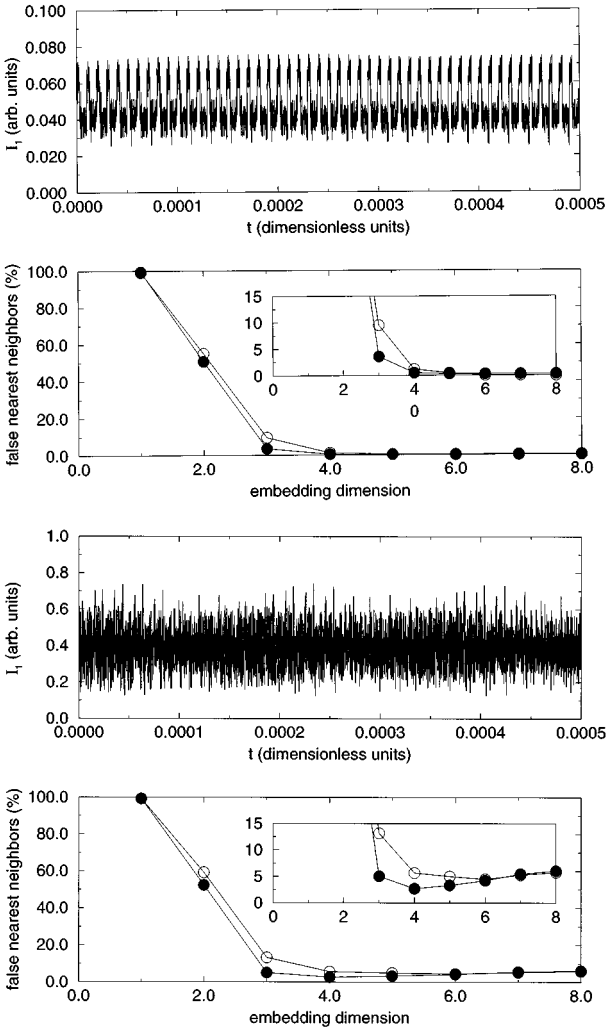

FIG. 16. Quasiperiodic time trace and its percentage of false nearest neighbors vs dimension. Full circles represent the numerical result, which corresponds to a pump rate of $q = 6 \times 10^5$ dimensionless units, ~ 1.1 times above threshold. Empty circles are the experimental result of Fig. 8(a). (b) Nonperiodic time trace and its percentage of false nearest neighbors vs dimension, which displays a residual percentage of FNNs, implying random dynamics. Full circles represent the numerical result, which corresponds to a pump rate of $q = 1 \times 10^6$ dimensionless units, ~ 2 times above threshold. In this case, the noise source strengths have been increased to a value of 1.2×10^{-4} dimensionless units to obtain better agreement with the experiments, which are represented by empty circles [from Fig. 8(b)].

IV. CONCLUSION

We have analyzed the fast, intracavity dynamics of an erbium-doped fiber laser in a ring cavity. Since it is well known that this kind of system presents interesting polarization dynamics, we have introduced a polarization controller inside the laser cavity. Self-pulsing has been observed in a very broad range of system configurations, both in the total output intensity of the laser and in the polarization-resolved dynamics, in periods of the order of the cavity round-trip time. In this regime the two different polarization modes can behave independently, i.e., one may show quasiperiodic dynamics and the other chaotic behavior, for instance. Due to the long cavity and fast detection devices, we have been able to sample the behavior inside a cavity round-trip. By carefully tuning the polarization controller, the self-pulsing behavior can be transformed into square-wave dynamics. In this case, the behavior of the two polarization modes is usually antiphase, as predicted for lasers with a strong multimode character. All these features can be reproduced by a stochastic delay-differential equation model, which takes into account the fact that a mean-field approximation in the propagation direction is misleading in this kind of long-cavity laser. Spontaneous emission is introduced via a noise term in the original Maxwell-Bloch equations and leads to a nontrivial stochastic contribution to the delay-differential model. This model is able to reproduce both the self-pulsing and the square-wave behavior. Spontaneous-emission noise is necessary to obtain the observed slow time drift of the patterns underlying the square-pulse structure. However, even though spontaneous emission (and hence the noise sources in the model) is always present in the laser operation, we observe, numerically and experimentally, both a deterministic and a noise-driven regime for slightly different values of the system parameters. The first situation corresponds to a quasiperiodic, low-dimensional motion and the second to a random, high-dimensional behavior. The coexistence of these two types of behavior in the same nonlinear dynamical system is a remarkable feature that deserves further study.

ACKNOWLEDGMENTS

We gratefully thank H. Abarbanel and C. Liu for making available to us the software on the false-nearest-neighbor method. We also acknowledge support from the Division of Chemical Sciences, Office of Basic Energy Sciences, Office of Energy Research, U.S. Department of Energy and the Office of Naval Research. J.G.O. acknowledges support from the Dirección General de Investigación Científica y Técnica (Spain).

[1] K. Otsuka, P. Mandel, S. Bielawski, D. Derozier, and P. Glorieux, Phys. Rev. A **46**, 1692 (1992).
[2] S. Bielawski, D. Derozier, and P. Glorieux, Phys. Rev. A **46**, 2811 (1992).
[3] E. Lacot, F. Stoeckel, and M. Chenevier, Phys. Rev. A **49**, 3997 (1994).
[4] P. Le Boudec, M. Le Flohic, P.L. François, F. Sanchez, and G. Stephan, Opt. Quantum Electron. **25**, 359 (1993).
[5] F. Sanchez, P. Le Boudec, P.L. François, and G. Stephan, Phys. Rev. A **48**, 2220 (1993).
[6] W.H. Loh, Y. Ozeki, and C.L. Tang, Appl. Phys. Lett. **56**, 2613 (1990).
[7] B. Meziane, F. Sanchez, G.M. Stephan, and P.L. François, Opt. Lett. **19**, 1970 (1994).
[8] W.H. Loh and C.L. Tang, IEEE J. Quantum Electron. **27**, 389 (1991).
[9] W.H. Loh and C.L. Tang, Opt. Commun. **85**, 283 (1991).
[10] Q.L. Williams and R. Roy, Opt. Lett. **21**, 1478 (1996).
[11] O. Svelto, *Principles of Lasers*, 3rd ed. (Plenum, New York, 1989).
[12] H.D.I. Abarbanel, R. Brown, J.J. Sidorowich, and L.S. Tsimring, Rev. Mod. Phys. **65**, 1331 (1993).
[13] A.M. Fraser and H.L. Swinney, Phys. Rev. A **33**, 1134 (1986).
[14] M.B. Kennel, R. Brown, and H.D.I. Abarbanel, Phys. Rev. A **45**, 3403 (1992).
[15] H.D.I. Abarbanel, Z. Gills, C. Liu, and R. Roy, Phys. Rev. A **53**, 440 (1996).
[16] K. Ikeda, Opt. Commun. **30**, 257 (1979).
[17] K. Ikeda, H. Daido, and O. Akimoto, Phys. Rev. Lett. **45**, 709 (1980).
[18] K. Otsuka and H. Iwamura, Phys. Rev. A **28**, 3153 (1983).
[19] J. García-Ojalvo and R. Roy, Phys. Lett. A (to be published).
[20] T.C. Gard, *Introduction to Stochastic Differential Equations* (Dekker, New York, 1987).